International Journal of Bifurcation and Chaos, Vol. 26, No. 1 (2016) 1630002 (17 pages)

DOI: 10.1142/S0218127416300020

Imaginary Scators Bound Set Under the Iterated Quadratic Mapping in $1 + 2$ Dimensional Parameter Space

M. Fernández-Guasti
Lab. de Óptica Cuántica, Depto. de Física,
Universidad A. Metropolitana – Iztapalapa,
09340 México D.F., Ap. Postal. 55-534, Mexico
mfg@xanum.uam.mx

Received November 30, 2014; Revised July 4, 2015

The quadratic iteration is mapped within a nondistributive imaginary scator algebra in $1 + 2$ dimensions. The Mandelbrot set is identically reproduced at two perpendicular planes where only the scalar and one of the hypercomplex scator director components are present. However, the bound three-dimensional **S** set projections change dramatically even for very small departures from zero of the second hypercomplex plane. The **S** set exhibits a rich fractal-like boundary in three dimensions. Periodic points with period m, are shown to be necessarily surrounded by points that produce a divergent magnitude after m iterations. The scator set comprises square nilpotent elements that ineluctably belong to the bound set. Points that are square nilpotent on the mth iteration, have preperiod 1 and period m. Two-dimensional plots are presented to show some of the main features of the set. A three-dimensional rendering reveals the highly complex structure of its boundary.

Keywords: 3D bifurcations; hypercomplex numbers; imaginary scators; quadratic iteration; Mandelbrot set; discrete dynamical systems.

1. Introduction

The iterated quadratic mapping satisfies the recurrence relationship $z_{n+1} = a_2 z_n^2 + a_1 z_n + c_0$, where the quantities z_n, c_0 are elements of a module and a_2, a_1 are elements of a ring. In real and complex algebra, the module and ring become fields, that is, sets with commutative group properties under the addition and product operations. In $\mathbb{R}$, the quadratic mapping gives rise to the logistic map, while in $\mathbb{C}$, the bound iterations define the Julia and Mandelbrot sets in dynamical and parameter space, respectively. These one- and two-dimensional cases are prototypical examples that exhibit continued bifurcation leading to chaos in discrete dynamical systems. The quadratic mapping can be extended to higher dimensions using other algebraic structures such as quaternions or Clifford algebras [Helmstetter & Micali, 2008], matrix algebras [Nascimento-Baptista *et al.*, 2012], nonassociative algebras, etc. Some of the field properties are necessarily lost in the generalization to higher dimensions. For example, quaternions and matrix algebras are no longer commutative and octonions are neither commutative nor associative. In some of these alternatives, such as hyperbolic complex numbers, the structure is no longer a division algebra, that is, not all elements have an inverse. Nonetheless, these algebraic structures are well suited for some physical scenarios such as Minkowski space-time [Catoni *et al.*, 2008].

There have been several efforts to extend two-dimensional fractal structures to higher dimensions.

For example, four-dimensional quaternion generalizations of the Mandelbrot and Julia sets [Gomatam *et al.*, 1995]. However, these mappings yield little new beyond the complex case [Bedding & Briggs, 1995]. On the other hand, there has been much less work in three-dimensional algebras compared with four or eight dimensions. The reason being that emphasis has been laid on division or normed algebras. The only possible division algebra, up to isomorphism, in dimension higher than two is four-dimensional (Frobenius theorem). However, if divisors of zero are permitted, the scope becomes much broader. There are some isolated proposals of three-dimensional number systems such as ternary algebra [Cheng & Tan, 2007] and triplex algebra [White & Nylander, 2009; Rama & Mishra, 2011] or variations of them [Bonzini, 2010] that render interesting bound sets under continued iteration. Visualizations of some of these sets, notably quasi-Fuschian fractals [Araki, 2006] and the Mandelbulb, have received wide dissemination [Aron, 2009; Sanderson, 2009]. The visualization of fractal geometry in three dimensions is quite challenging and has become a specialized study of programmers and developers. Methods originated in geographic visualization, architecture and digital animation are proving quite useful to render these rather complicated structures [Blackledge, 2002].

In the present approach, the three-dimensional product and addition operations of imaginary scator algebra are invoked to appraise the quadratic mapping. The algebra is akin to the subset of paravectors in Clifford algebras where numbers contain a scalar and a vector part. However, it differs from Cliffordian structures among other things, because although it is equipped with an order parameter, this quantity does not have an associated bilinear form. Scator elements can be viewed as hypercomplex numbers in $1+n$ dimensions. They have n copies of the complex numbers set embedded in the higher dimensional set, all sharing the real part of the hypercomplex number. If all but one of the scator director components is nonvanishing, the complex plane is recovered [Fernández-Guasti & Zaldívar, 2013a]. Imaginary scator algebra is a finite dimensional algebra over the reals with a multiplicative identity. It is thus a hypercomplex algebra in the sense of Kantor and Solodovnikov except for the distributivity condition that is commonly requested [Kantor & Solodovnikov, 1989]. In general, the scator product does not distribute over addition. However, the scator product is commutative and all elements in the scator set have an inverse, except zero. Nonetheless, scator algebra is no longer a division algebra because it has zero products of nonzero factors. In particular, nilpotent elements exist when the two factors are equal. Nonetheless, as we shall presently see, this restriction does not prevent the imaginary scator number system from generating consistent iterated mappings.

The structure of this manuscript is as follows: In Sec. 2, the necessary elements of imaginary scator algebra in $1+2$ dimensions are introduced. Emphasis is laid on the squaring function and the nilpotent conditions. The quadratic iteration with imaginary scator numbers is presented in Sec. 3. In Sec. 4, one of the salient features of the 3D fractal is discussed: Periodic points have a vicinity that produce a scator with divergent magnitude. Points that are eventually square nilpotent are discussed in Sec. 5. Section 5.1 establishes the lack of an upper limit for the scator magnitude bound points. The elementary symmetries of the three-dimensional set are discussed in Sec. 6. Conclusions are drawn in the last section.

2. Imaginary Scators

Imaginary scator elements, sometimes referred to as elliptic scators, in $1+2$ dimensions can be written in terms of three real numbers $\overset{o}{\varphi} = (s; x, y)$, $s, x, y \in \mathbb{R}$. The first component, named the *scalar component*, stands on a different ground from other components. To stress this fact, it is separated by a semi-colon from the rest. Subsequent components are named *director components*. They are not referred to as a "vector part" because vectors are not a subset of the scator set [Fernández-Guasti & Zaldívar, 2013b]. Scator elements are decorated with an oval placed overhead.[1] Scators can be represented in terms of a basis, $\overset{o}{\varphi} = s + x\check{\mathbf{e}}_x + y\check{\mathbf{e}}_y$, where $\check{\mathbf{e}}_x, \check{\mathbf{e}}_y \notin \mathbb{R}$. *Addition* of scators is defined by the sum of each component $\overset{o}{\alpha} + \overset{o}{\beta} = (a_0 + a_1\check{\mathbf{e}}_x + a_2\check{\mathbf{e}}_y) + (b_0 + b_1\check{\mathbf{e}}_x + b_2\check{\mathbf{e}}_y) = (a_0 + b_0) + (a_1 + b_1),\ \check{\mathbf{e}}_x + (a_2 + b_2)\check{\mathbf{e}}_y$. The scator set is a commutative group under addition. The *product* operation of scators

[1] \overset{o} in LaTeX lore.

$\overset{o}{\alpha} = (a_0; a_1, a_2)$, $\overset{o}{\beta} = (b_0; b_1, b_2)$, is defined by

$$\begin{aligned}\overset{o}{\alpha}\overset{o}{\beta} &= a_0 b_0 \left(1 - \frac{a_1 b_1}{a_0 b_0}\right)\left(1 - \frac{a_2 b_2}{a_0 b_0}\right) \\ &\quad + (a_0 b_1 + b_0 a_1)\left(1 - \frac{a_2 b_2}{a_0 b_0}\right)\check{\mathbf{e}}_x \\ &\quad + (a_0 b_2 + b_0 a_2)\left(1 - \frac{a_1 b_1}{a_0 b_0}\right)\check{\mathbf{e}}_y. \qquad (1)\end{aligned}$$

This definition departs from the real scator product definition and establishes a different topology [Fernández-Guasti & Zaldívar, 2013a]. This state of affairs is analogous to the differences that arise between complex algebra ($i^2 = -1$) and hyperbolic numbers algebra ($i^2 = 1$) due to the product definition of two imaginary units as minus one or one respectively. The *product* operation of two equal imaginary scators, that is, the square of an imaginary scator $\overset{o}{\varphi} = (s; x, y)$ is then

$$\begin{aligned}\overset{o}{\varphi}^2 &= (s + x\check{\mathbf{e}}_x + y\check{\mathbf{e}}_y)^2 \\ &= (s_\diamond; x_\diamond, y_\diamond) \\ &= s_\diamond + x_\diamond\check{\mathbf{e}}_x + y_\diamond\check{\mathbf{e}}_y, \\ \overset{o}{\varphi}^2 &= \left(s^2 - x^2 - y^2 + \frac{x^2y^2}{s^2}\right) \qquad (2) \\ &\quad + \left(2sx - \frac{2xy^2}{s}\right)\check{\mathbf{e}}_x \\ &\quad + \left(2sy - \frac{2yx^2}{s}\right)\check{\mathbf{e}}_y.\end{aligned}$$

If $y = 0$, $\overset{o}{\varphi}^2 = (s + x\check{\mathbf{e}}_x)^2 = (s^2 - x^2) + (2sx)\check{\mathbf{e}}_x$, or, if $x = 0$ in (2), $\overset{o}{\varphi}^2 = (s + y\check{\mathbf{e}}_y)^2 = (s^2 - y^2) + (2sy)\check{\mathbf{e}}_y$, we recover the complex algebra product. From these last two equations if $s = 0$, and $x = 1$ or $y = 1$ respectively, the square of the hyperimaginary units are $\check{\mathbf{e}}_x^2 = -1$ and $\check{\mathbf{e}}_y^2 = -1$. An inverted hat or check is used to decorate unit director components in imaginary scators versus the hat used to label them in real scator algebra. From the symmetry of the x and y variables, it is clear that the two hyperimaginary axes are equivalent. Two copies of the complex plane are embedded in $1 + 2$ imaginary scator algebra, sharing the scalar axis and having two distinct but equivalent hypercomplex axes. From the product of two different scators (1), it can be seen that $(s + x\check{\mathbf{e}}_x)(s + y\check{\mathbf{e}}_y) = s^2 + sx\check{\mathbf{e}}_x + sy\check{\mathbf{e}}_y$. If $s = 0$ and $x = y = 1$, then $\check{\mathbf{e}}_x\check{\mathbf{e}}_y = 0$. Thus, due to the addition and product properties, the two hypercomplex axes can be visualized as orthogonal axes. However, due to the lack of distributivity, the relationships $\check{\mathbf{e}}_x\check{\mathbf{e}}_y = -\delta_{xy}$ are not sufficient to establish the product operation rules.

To insure consistency, different component limits are taken in succession, evaluated first for the director components variables in any order, and thereafter, evaluating the scalar component limit. For example, if $x = 0$ and $s = 0$, the limit on the director component variable $x \to 0$ is taken first $s_\diamond + x_\diamond\check{\mathbf{e}}_x + y_\diamond\check{\mathbf{e}}_y = (s^2 - y^2) + 2sy\check{\mathbf{e}}_y$, and then the scalar variable limit $s \to 0$ is evaluated, thus $s_\diamond + x_\diamond\check{\mathbf{e}}_x + y_\diamond\check{\mathbf{e}}_y = -y^2$. This criterion is extended to all other functional relationships.

The *conjugate* of a scator $\overset{o}{\varphi} = s + x\check{\mathbf{e}}_x + y\check{\mathbf{e}}_y$ is defined by the negative of the director components, while the scalar component remains unchanged $\overset{o}{\varphi}^* = s - x\check{\mathbf{e}}_x - y\check{\mathbf{e}}_y$. The square magnitude of a scator $\|\overset{o}{\varphi}\|^2$ is equal to the scator times its conjugate

$$\|\overset{o}{\varphi}\|^2 = \overset{o}{\varphi}\overset{o}{\varphi}^* = s^2 + x^2 + y^2 + \frac{x^2y^2}{s^2}. \qquad (3)$$

This quantity is real and can thus be used as an order parameter. It will be employed to establish the bound criterion in the quadratic mapping. The multiplicative inverse of $\overset{o}{\varphi}$ is

$$\overset{o}{\varphi}^{-1} = \frac{1}{s^2\left(1 + \frac{x^2}{s^2}\right)\left(1 + \frac{y^2}{s^2}\right)}\overset{o}{\varphi}^*. \qquad (4)$$

From the above expression, $\overset{o}{\varphi}$ is always invertible except if all components are zero or if $s = 0$ when $xy \neq 0$.

The subspace $\mathbb{E}^{1+2} \subset \mathbb{R}^3$, where the scator magnitude (3) is finite, is defined by

$$\mathbb{E}^{1+2} = \{\overset{o}{\varphi} = s + x\check{\mathbf{e}}_x + y\check{\mathbf{e}}_y : s \neq 0 \text{ if } x, y \neq 0\}, \qquad (5)$$

that is, the scalar component should not be zero if the two director components are finite. Let the extended set $\overline{\mathbb{E}}^{1+2}$ be defined in a similar fashion as the extended complex plane but adding one more dimension; That is, the *extended scator set*

$$\overline{\mathbb{E}}^{1+2} = \mathbb{E}^{1+2} \cup \{\overset{o}{\varphi} : \|\overset{o}{\varphi}\|^2 = \infty\} = \mathbb{R}^3 \cup \{\infty\}, \qquad (6)$$

involves three dimensions and includes the points at infinity. The points at infinity are obtained by letting any of the scator components tend to infinity, that is, $\|\overset{o}{\varphi}\|^2 \to \infty$ if $s \to \infty$ and/or $x \to \infty$ and/or $y \to \infty$. Extensions of complex algebra to higher dimensions equipped with a quadratic norm, impose this type of condition. Namely, the points at infinity require that at least one of the components tends to infinity. However, there is also another possibility in scator algebra. If s becomes very small while x, y are both different from zero, the magnitude of the scator, from the magnitude definition (3), becomes very large. There is then a set of points on the x, y plane whose magnitude approaches infinity

$$\mathbf{R}_s = \Big\{ s + x\check{\mathbf{e}}_x + y\check{\mathbf{e}}_y \in \overline{\mathbb{E}}^{1+2} : x \neq 0, y \neq 0, \\ \|(s; x, y)\| \underset{s\to 0}{\longrightarrow} \infty \Big\}. \tag{7}$$

This set, also present in real scator algebra, is depicted in Fig. 1 of reference [Fernández-Guasti, 2014]. It includes all points of the plane $s = 0$, except for the two, on axis straight lines.

Definition 2.1. The point $s_0 + x_0\check{\mathbf{e}}_x + y_0\check{\mathbf{e}}_y$ has a *divergent vicinity* if there exists a set of points $(s_0+\delta s)+(x_0+\delta x)\check{\mathbf{e}}_x+(y_0+\delta y)\check{\mathbf{e}}_y$ for infinitesimal $\delta s, \delta x, \delta y \in \mathbb{R}$, whose magnitude tends to infinity $\|(s_0 + \delta s) + (x_0 + \delta x)\check{\mathbf{e}}_x + (y_0 + \delta y)\check{\mathbf{e}}_y\| \to \infty$.

The point $(0; 0, 0)$ has a divergent vicinity since the magnitude of $(0; 0 + \delta x, 0 + \delta y)$ is infinite. Furthermore, all points with infinitesimal scalar and arbitrary nonvanishing director components $(\delta s; x, y)$ have a divergent vicinity since the magnitude of points $(\delta s - \delta s; x + \delta x, y + \delta y)$ is infinite. The only points with finite magnitude within the x, y plane at $s = 0$ are those lying on the axes lines $x = 0$ or $y = 0$.

Lemma 1. *The only nontrivial square nilpotent elements in $1 + 2$ dimensional imaginary scator algebra are elements whose three components have equal absolute value.*

Proof. A scator element is zero if and only if, all its components are zero, i.e. $\overset{o}{\varphi} = 0 \Leftrightarrow \overset{o}{\varphi} = (0; 0, 0)$. A nonzero element is nilpotent if $\overset{o}{\varphi}^n = 0$ for some $n \in \mathbb{N}$. In particular, a scator element is square nilpotent if $\overset{o}{\varphi}^2 = (s_\diamond; x_\diamond, y_\diamond) = (0; 0, 0)$. The square function components (2), can be factored as

$$\begin{aligned} \overset{o}{\varphi}^2 &= s_\diamond + x_\diamond\check{\mathbf{e}}_x + y_\diamond\check{\mathbf{e}}_y \\ &= s^2\left(1 - \frac{x^2}{s^2}\right)\left(1 - \frac{y^2}{s^2}\right) + 2sx\left(1 - \frac{y^2}{s^2}\right)\check{\mathbf{e}}_x \\ &\quad + 2sy\left(1 - \frac{x^2}{s^2}\right)\check{\mathbf{e}}_y. \end{aligned} \tag{8}$$

Since all scator components of the squared function must be zero, then the required conditions are $x^2 = s^2$ and $y^2 = s^2$. The absolute value of the director components have to be equal to the scalar component. ■

Corollary 2.1. *The square of an invertible element is invertible if it is not square nilpotent.*

Proof. All imaginary scator elements in $\mathbb{E}^{1+2}$ have inverse except zero. The square of a nonzero element is then invertible if it is different from zero. ■

3. Iterated Quadratic Mapping

Consider the family of maps $P_c : \overset{o}{\varphi} \mapsto \overset{o}{\varphi}_0^2 + \overset{o}{c}$ from $\overline{\mathbb{E}}^{1+2}$ to $\overline{\mathbb{E}}^{1+2}$, where the variable $\overset{o}{\varphi}$ and the constant $\overset{o}{c}$ are now scator elements. P_c is a quadratic mapping in the sense that it involves the evaluation of the square function plus a constant. The *square function* q, is defined by the product of two arbitrary elements in the algebra when the two factors are equal. It is also a quadratic mapping over $\mathbb{R}$ in the following sense

Lemma 2. *The square function mapping $q : \overset{o}{\varphi} \mapsto \overset{o}{\varphi}_0^2$ from $\overline{\mathbb{E}}^{1+2}$ to $\overline{\mathbb{E}}^{1+2}$ satisfies $q(\lambda\overset{o}{\varphi}) = \lambda^2 q(\overset{o}{\varphi})$, $\lambda \in \mathbb{R}$.*

Proof. A scalar $\lambda \in \mathbb{R}$ is an imaginary scator with all director components equal to zero, i.e. $\overset{o}{\lambda} = \lambda + 0\check{\mathbf{e}}_x + 0\check{\mathbf{e}}_y$, $\overset{o}{\lambda} \in \overline{\mathbb{E}}^{1+2}$. That is, real algebra is embedded in scator algebra. Although in general, the product does not distribute over addition, in the particular case of a scalar times an arbitrary scator, the scalar does distribute over the scator components [Fernández-Guasti & Zaldívar, 2013b]. This result can be seen from (1), by letting $a_0 = \lambda$, $a_1 = a_2 = 0$. Therefore, $\lambda\overset{o}{\varphi} = \lambda s + \lambda x\check{\mathbf{e}}_x + \lambda y\check{\mathbf{e}}_y$ for all $\lambda \in \mathbb{R}$ and for all $\overset{o}{\varphi}$ in $\overline{\mathbb{E}}^{1+2}$. From (8),

$$q(\lambda\overset{o}{\varphi}) = \lambda^2 s^2\left(1 - \frac{\lambda^2 x^2}{\lambda^2 s^2}\right)\left(1 - \frac{\lambda^2 y^2}{\lambda^2 s^2}\right)$$

$$+2\lambda s\lambda x\left(1-\frac{\lambda^2y^2}{\lambda^2s^2}\right)\check{\mathbf{e}}_x$$

$$+2\lambda s\lambda y\left(1-\frac{\lambda^2x^2}{\lambda^2s^2}\right)\check{\mathbf{e}}_y.$$

Since λ^2 is a scalar, it can be factored from the above scator components

$$q(\lambda\overset{o}{\varphi})=\lambda^2\left[s^2\left(1-\frac{x^2}{s^2}\right)\left(1-\frac{y^2}{s^2}\right)\right.$$
$$\left.+2sx\left(1-\frac{y^2}{s^2}\right)\check{\mathbf{e}}_x+2sy\left(1-\frac{x^2}{s^2}\right)\check{\mathbf{e}}_y\right].$$

Therefore $q(\lambda\overset{o}{\varphi})=\lambda^2q(\overset{o}{\varphi})$. ■

In abstract algebra, it is customary to introduce the associated mapping $b_q:\mathbb{E}^{1+2}\times\mathbb{E}^{1+2}\to\mathbb{E}^{1+2}$ defined by $b_q(\overset{o}{\alpha},\overset{o}{\beta})=q(\overset{o}{\alpha}+\overset{o}{\beta})-q(\overset{o}{\alpha})-q(\overset{o}{\beta})$. Some authors [Helmstetter & Micali, 2008, Chapter 2] request that the associated mapping should also be $\mathbb{R}$ bilinear in a quadratic mapping. This criterion is not fulfilled in scator algebra, $b_q(\lambda\overset{o}{\alpha},\overset{o}{\beta})\neq\lambda b_q(\overset{o}{\alpha},\overset{o}{\beta})$ and $b_q(\overset{o}{\alpha},\lambda\overset{o}{\beta})\neq\lambda b_q(\overset{o}{\alpha},\overset{o}{\beta})$. The Mandelbrot-like set is obtained by fixing the initial point $\overset{o}{\varphi}_0=(0;0,0)$ and varying the parameter $\overset{o}{c}$. Bound points obtained by iteration of this procedure comprise the corresponding M-set in $\overline{\mathbb{E}}^{1+2}$. The confined set in parameter space for imaginary scators in $1+2$ dimensions is given by

$$\mathbf{S}=\{\overset{o}{c}\in\overline{\mathbb{E}}^{1+2}:m\in\mathbb{N},\|P_c^{\circ m}(0)\|\nrightarrow\infty\},\quad(9)$$

where $P_c:\overset{o}{\varphi}\mapsto\overset{o}{\varphi}^2+\overset{o}{c}$, $P_c^{\circ m}$ denotes the *m-fold composition* $P_c^{\circ m}=P_c\circ P_c\circ\cdots\circ P_c$ of the function P_c with itself and the 0 argument in $P_c^{\circ m}(0)$ means that the function is initially evaluated at zero. A two-dimensional rendering of this set at a constant second hyperimaginary plane is shown in Fig. 1. The picture is reminiscent of the Mandelbrot set although the main cardioid as well as the bulbs are squeezed. Similar maps are obtained even for tiny departures from zero in the second hyperplane. Values as low as $y=10^{-40}$ already show this squeezing behavior. At these very small coordinate values, care has to be taken regarding the precision of the numerical calculations. The iterated function satisfies the recurrence relationship $\overset{o}{\varphi}_{m+1}=\overset{o}{\varphi}_m^2+\overset{o}{c}$, where the subindex stands for the iteration number.

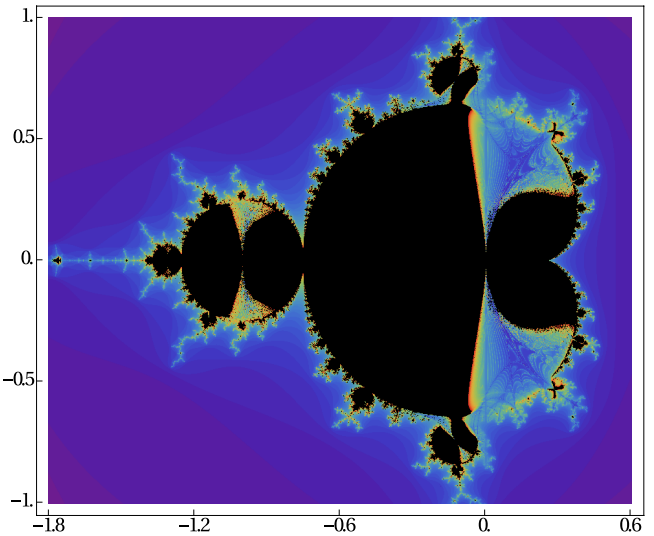

Fig. 1. Two-dimensional rendering of the $\mathbf{S}$ set in $\overline{\mathbb{E}}^{1+2}$ $(s;x,10^{-7})$. The abscissa corresponds to the scalar (or real) s axis, $-1.8<s<0.6$, while the ordinate depicts a director component, say the hyperimaginary x axis $(-1<x<1)$. The other hyperimaginary director component (y axis), is coming out of the page. The $\mathbf{S}$ set is evaluated at a constant $y=10^{-7}$ hyperplane.

For $\overset{o}{c}=s+x\check{\mathbf{e}}_x+y\check{\mathbf{e}}_y$, the quadratic iteration recurrence relationship for the scalar component is

$$s_{m+1}=s_m^2\left(1-\frac{x_m^2}{s_m^2}\right)\left(1-\frac{y_m^2}{s_m^2}\right)+s\quad(10a)$$

and for the director components, the recurrence relationships are

$$x_{m+1}=2s_mx_m\left(1-\frac{y_m^2}{s_m^2}\right)+x,\quad(10b)$$

$$y_{m+1}=2s_my_m\left(1-\frac{x_m^2}{s_m^2}\right)+y.\quad(10c)$$

4. Divergent Magnitude Set in the Vicinity of Periodic Points

4.1. *Periodic points*

Periodicity is defined in an analogous fashion as in complex dynamics [Blanchard, 1984, p. 88].

Definition 4.1. If $\overset{o}{\varphi}_m=\overset{o}{\varphi}_0$ for some m, then $\overset{o}{\varphi}_0$ is a periodic point and $O^+(\overset{o}{\varphi}_0)$ is a periodic orbit. If m is the first positive integer such that $\overset{o}{\varphi}_m=\overset{o}{\varphi}_0$, then m is the period of the orbit. A point $\overset{o}{\varphi}$ is *eventually periodic* if, for some m, $P^{\circ m}(\overset{o}{\varphi})$ is a periodic point. The point $\overset{o}{\varphi}$ is *preperiodic* if it is eventually periodic but not periodic yet.

If the period of an orbit is 1, $\overset{o}{\varphi}_0$ is a fixed point. The origin $\overset{o}{\varphi}_0 = \overset{o}{c}_0 = 0 + 0\check{\mathbf{e}}_x + 0\check{\mathbf{e}}_y$ is clearly a fixed point in the scator quadratic mapping. In parameter space, the initial point is always $\overset{o}{\varphi}_0 = 0 + 0\check{\mathbf{e}}_x + 0\check{\mathbf{e}}_y$. The first iteration gives the additive constant $\overset{o}{\varphi}_1 = \overset{o}{c} = s + x\check{\mathbf{e}}_x + y\check{\mathbf{e}}_y$. If $s = 0$ and $x \neq 0, y \neq 0$, the scator magnitude becomes infinite. The divergent $\mathbf{R}_s$ plane is thus obtained and is depicted as a vertical line in the s, x plane for constant $y = 10^{-7}$, as shown in Fig. 3. The $\overset{o}{\varphi}_0 = \overset{o}{c}_0 = 0 + 0\check{\mathbf{e}}_x + 0\check{\mathbf{e}}_y$ fixed point thus has a divergent vicinity. This $\mathbf{R}_s$ plane (in yellow) produces a squeezing of the M-set main cardioid illustrated in Fig. 4.

4.2. *Second iteration*

The second iteration for the scalar is

$$s_2 = s^2\left(1 - \frac{x^2}{s^2}\right)\left(1 - \frac{y^2}{s^2}\right) + s \tag{11a}$$

and for the director components

$$x_2 = 2sx\left(1 - \frac{y^2}{s^2}\right) + x, \quad y_2 = 2sy\left(1 - \frac{x^2}{s^2}\right) + y. \tag{11b}$$

The cycle 2 periodic points in parameter space impose $\overset{o}{\varphi}_2 = \overset{o}{\varphi}_0 = 0$. The simultaneous equations that ought to be fulfilled are then $s_2 = 0$, $x_2 = 0$ and $y_2 = 0$. If $x = y = 0$, from (11a), $s = 0$ or $s = -1$. If $x = 0$, $y \neq 0$, from the second equation in (11b), $s = -\frac{1}{2}$; substitution of $x = 0$ in (11a) gives $y = \pm\sqrt{s^2 + s}$ and from the previous result $y = \pm\frac{i}{2}$, where $i^2 \equiv -1$ ($x \neq 0, y = 0$ gives an analogous result for x). If $x \neq 0$, $y \neq 0$, from (11b), $y = \pm\sqrt{s^2 + s/2}$ and $x = \pm\sqrt{s^2 + s/2}$. Substitution of these expressions in (11a) gives $s = -\frac{1}{4}$, and this result back in the previous two equations gives $x = y = \pm\frac{i}{4}$. The two solutions with real coefficients are $\overset{o}{c} = 0 + 0\check{\mathbf{e}}_x + 0\check{\mathbf{e}}_y$ and $\overset{o}{c} = -1 + 0\check{\mathbf{e}}_x + 0\check{\mathbf{e}}_y$. The other eight possibilities have complex solutions: $-\frac{1}{4} \pm \frac{1}{4}i\check{\mathbf{e}}_x \pm \frac{1}{4}i\check{\mathbf{e}}_y$, $-\frac{1}{2} \pm \frac{1}{2}i\check{\mathbf{e}}_x + 0\check{\mathbf{e}}_y$, $-\frac{1}{2} + 0\check{\mathbf{e}}_x \pm \frac{1}{2}i\check{\mathbf{e}}_y$, but the scator coefficients must be real. Therefore, there are no period 2 points lying outside the scalar axis.

Due to s terms in the denominators, all three components in iteration (11a) and (11b) become large for nonzero director components if the scalar becomes small. Consider the points that on the second iteration map into the $\mathbf{R}_s$ set, whose magnitude tends to infinity. That is, points where the scalar component becomes zero while the director components are nonzero, $x_2 \neq 0$, $y_2 \neq 0$. Only the equation for the scalar component $s_2 = 0$ is imposed,

$$s^4 + s^3 - (x^2 + y^2)s^2 + x^2y^2 = 0. \tag{12}$$

Since there are three independent variables, this equation represents a 2D surface embedded in 3D space. Points on this surface, depicted in Fig. 2, yield infinite magnitude scators on the second iteration provided that $x_2, y_2 \neq 0$. The points within this surface clearly do not belong to the $\mathbf{S}$ set. If one of the director variables is fixed, for example, when a plane with constant director component is analyzed, their intersection produces a (1D) curve embedded in 3D space. Consider a plane where $y \ll s, x$. Equation (12) can be approximated to $s^2 - x^2 + s \approx 0$. The terms involving s can be collected as $s^2 + s = (s + \frac{1}{2})^2 - \frac{1}{4}$. The equation is then $(s + \frac{1}{2})^2 - x^2 = \frac{1}{4}$, a rectangular hyperbola with center at $(-\frac{1}{2}; 0, 0)$ and focii at $-1/2 \pm 1/\sqrt{2}$. This hyperbola intersects the scalar axis at 0 and -1 as shown on the right graph of the middle row in Fig. 3. However, as we saw earlier, there is a periodic point

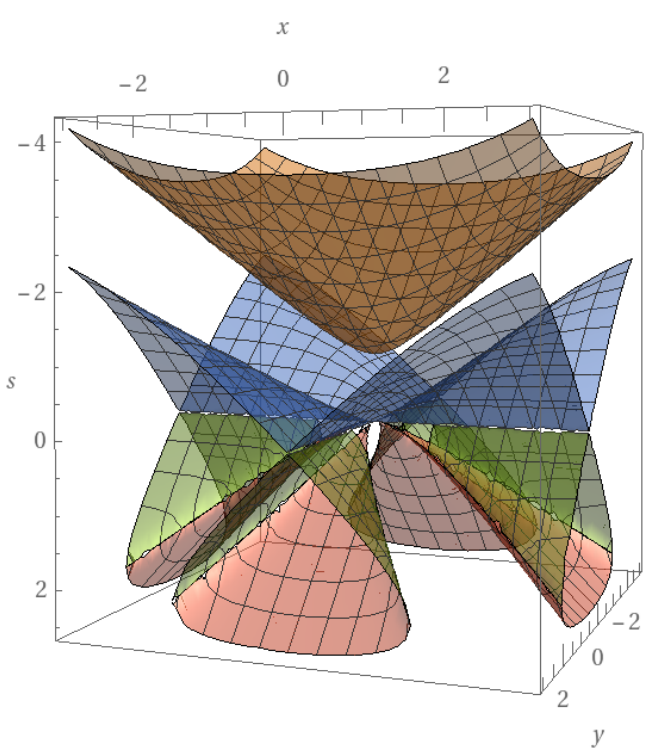

Fig. 2. Points on surfaces given by Eq. (12) produce a divergent magnitude on the second iteration.

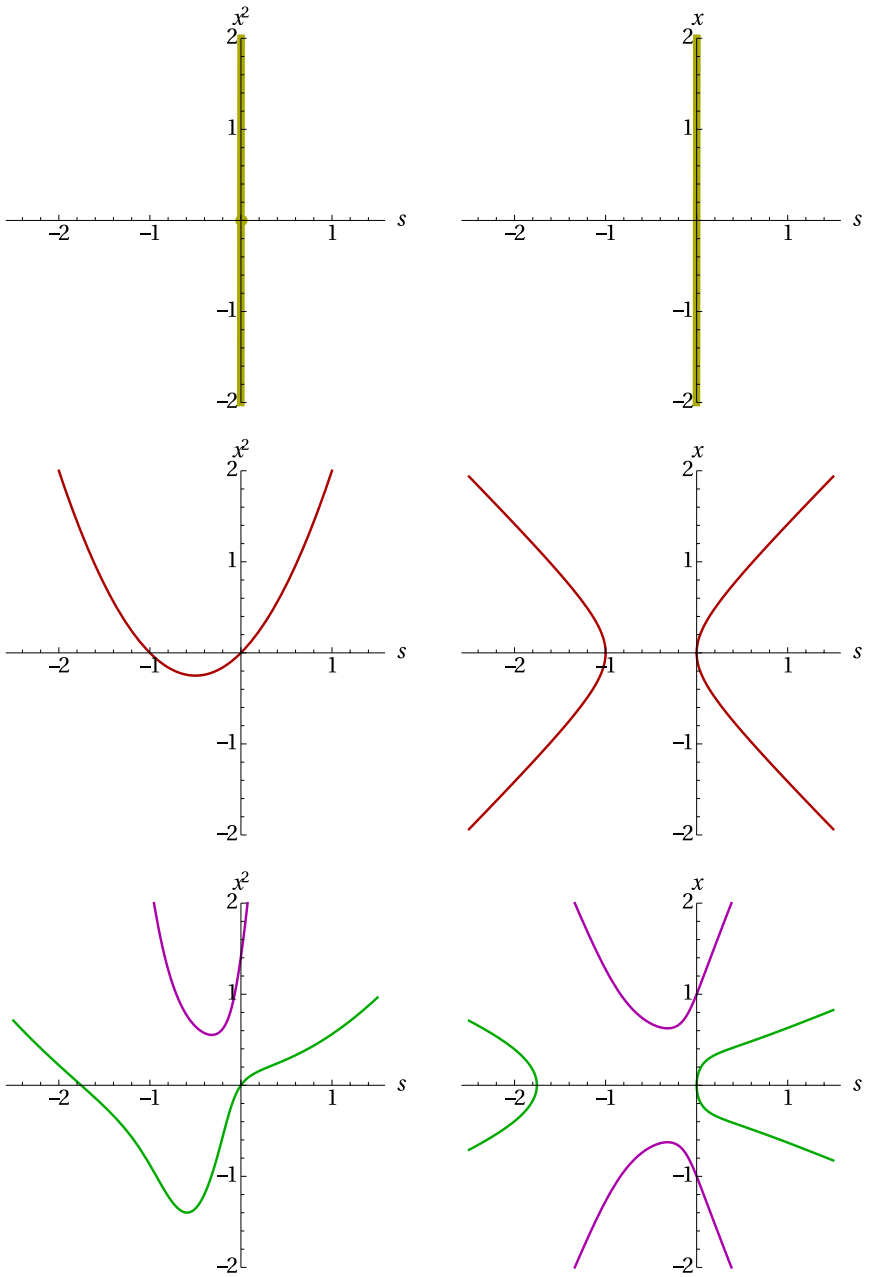

Fig. 3. Polynomials (from top to bottom), $s = 0$, $s^2 - x^2 + s = 0$ and $x^4 - (6s^2 + 6s + 1)x^2 + (s^4 + 2s^3 + s^2 + s) = 0$. Plots of x^2 as a function of s are shown on the LHS. The corresponding plots for x as a function of s are shown on the RHS. Along these curves, the scator magnitude becomes infinite in the first (top row), second (middle) or third (bottom) iteration.

at $\overset{o}{c} = -1 + 0\check{\mathbf{e}}_x + 0\check{\mathbf{e}}_y$. Furthermore, from real analysis we know that there is a period 2 fixed point at -1 with its concomitant basin of attraction.

Consider a point in the vicinity of -1, $s = -1 + \delta s$, where $|\delta s| \ll 1$. Evaluate the polynomial (12) with $s \to -1 + \delta s$, $x \to \delta x$, $y \to \delta y$ recalling that $s^n = (-1)^n + (-1)^{n-1} n\delta s + \cdots$,

$$\delta s = \frac{\delta x^2 \delta y^2 - (\delta x^2 + \delta y^2)}{1 - 2(\delta x^2 + \delta y^2)}.$$

If $\delta x^2, \delta y^2 \ll 1$, then $\delta s \approx -(\delta x^2 + \delta y^2)$. The point $\overset{o}{c} + \overset{o}{\delta} = -(1 + \delta x^2 + \delta y^2) + \delta x \check{\mathbf{e}}_x + \delta y \check{\mathbf{e}}_y$ lies in the vicinity of the point $\overset{o}{c} = -1 + 0\check{\mathbf{e}}_x + 0\check{\mathbf{e}}_y$. The quadratic iteration of this point evaluated to lowest order in $\delta x, \delta y$ is $P_c(-(1 + \delta x^2 + \delta y^2) + \delta x \check{\mathbf{e}}_x + \delta y \check{\mathbf{e}}_y) = 0 - \delta x \check{\mathbf{e}}_x - \delta y \check{\mathbf{e}}_y$, since $s^2 \approx 1 + 2\delta x^2 + 2\delta y^2$ and thus $s^2 - \delta x^2 - \delta y^2 + s \approx 0$. But this $0 - \delta x \check{\mathbf{e}}_x - \delta y \check{\mathbf{e}}_y$ point has an infinite magnitude. Therefore, the period 2 point $-1 + 0\check{\mathbf{e}}_x + 0\check{\mathbf{e}}_y$ has a vicinity

$-(1+\delta x^2+\delta y^2)+\delta x\check{\mathbf{e}}_x+\delta y\check{\mathbf{e}}_y$ that maps to $\mathbf{R}_s$ on the second iteration. The hyperbola (drawn in red) leading to infinite magnitude in the second iteration is superimposed on the bound set in Fig. 4. The main cardioid is squeezed at the origin due to the right branch of the hyperbola. Since $0+0\check{\mathbf{e}}_x+0\check{\mathbf{e}}_y$ is a solution to $s_n=0$ for all n, there is always a curve intersecting the scalar axis at the origin. The largest bulb to its left, is also squeezed at its center located at -1, the period 2 point where the left branch of the hyperbola intersects the scalar axis.

4.3. *Third iteration*

The cycle 3 periodic points in parameter space impose $\overset{o}{\varphi}_3=0$. The simultaneous equations that ought to be fulfilled are then $s_3=0$, $x_3=0$ and $y_3=0$. Analytic solutions for the general case are not possible because eighth order polynomials are now involved. Dropping out a director component lowers the single variable polynomial order by two. The equation for the scalar component $s_3=0$ in a plane where $y\ll s,x$ is approximately $s_2^2-x_2^2+s\approx 0$. With the aid of (11a) and (11b), this expression can be written in standard polynomial form for the hypercomplex director variable x,

$$x^4-(6s^2+6s+1)x^2 + (s^4+2s^3+s^2+s)=0. \tag{13}$$

The four solutions to this equation, plotted in the lower row of Fig. 3, are

$$x=\pm\frac{\sqrt{1+6s+6s^2\pm\sqrt{1+8s+44s^2+64s^3+32s^4}}}{\sqrt{2}}.$$

Two solutions intersect the scalar axis at 0 and $-1.7548\ldots$, the latter being the location of the period 3 point on the real axis. The other two solutions do not intersect the scalar axis. The off axis period 3 points in the s,x plane are approximately $-0.122\pm 0.744\check{\mathbf{e}}_x$. Points that belong to the curves

$$s\pm\frac{\sqrt{1+6s+6s^2\pm\sqrt{1+8s+44s^2+64s^3+32s^4}}}{\sqrt{2}}\check{\mathbf{e}}_x+\delta y\check{\mathbf{e}}_y,$$

generate divergent magnitude scators on the third iteration. In Fig. 4, these curves are superimposed on the $\mathbf{S}$ set evaluated at the hyperplane $\delta y=10^{-7}$. The left most curve (in green) intersects the scalar axis close to -1.75 where the center of the main cardioid of the largest copy of the M-set is located as can be guessed from Fig. 4. The remaining two solutions (in magenta) intersect the off scalar axis period 3 bulbs at their centers $(-0.122\pm 0.744\check{\mathbf{e}}_x)$ producing a skew squeezing. If δy is strictly zero, these curves no longer produce divergent magnitudes (thus not present in the M-set).

All bulbs suffer the same fate, a squeezing at their centers where the mth periodic point is located. There are surfaces similar to those depicted in Fig. 2 for higher order polynomials. They intersect each of the m centers and produce infinite magnitude scators after the mth iteration. At the intersection of these surfaces with a plane, curves similar to those depicted in Fig. 4 are produced.

Let us generalize these assertions in the following proposition:

Proposition 1. *For every m periodic scator point under the quadratic iteration mapping from $\overline{\mathbb{E}}^{1+2}$*

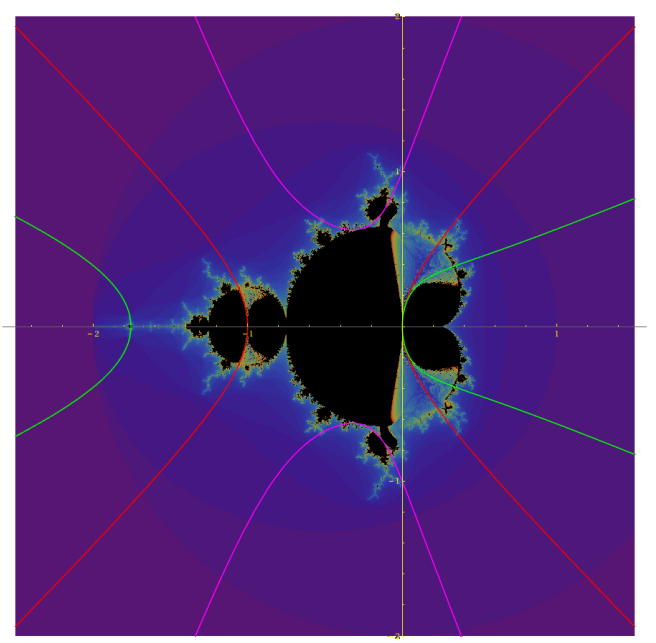

Fig. 4. Divergent magnitude curves: one iteration (yellow), two iterations (red), three iterations, intersecting the scalar axis (green) and off axis (magenta). There are four hyperplanes that produce this same set: $y=\pm\delta$ and $x=\pm\delta$, where $\delta=10^{-7}$.

to $\overline{\mathbb{E}}^{1+2}$ in parameter space, there is a vicinity that produces a scator with divergent magnitude in the mth iteration.

Proof. Periodic points with period m require that $\overset{o}{\varphi}_m = 0$, that is, the point represented by the scator $\overset{o}{\varphi}_1 = \overset{o}{c}$ returns to zero after m iterations. The periodicity condition $\overset{o}{\varphi}_m = s_m + x_m\check{\mathbf{e}}_x + y_m\check{\mathbf{e}}_y = 0 + 0\check{\mathbf{e}}_x + 0\check{\mathbf{e}}_y$, involves three equations in $1+2$ dimensions. Namely $s_m = 0$, $x_m = 0$ and $y_m = 0$. Let the solution to these three equations in terms of the initial variables be $\overset{o}{\varphi}_1 = \overset{o}{c} = s(m, r_s) + x(m, r_x)\check{\mathbf{e}}_x + y(m, r_y)\check{\mathbf{e}}_y$, where the notation $s(m, r_s)$ refers to the values of s for the mth iteration and $r_s \leq m$ is the r_sth root. The notation for the director coefficients $x(m, r_x), y(m, r_y)$ follow a similar convention. The solutions have been labeled with different subindices in r because any of the m^3 combinations between them is possible.

A divergent magnitude is obtained when the scalar component of the mth iteration scator is zero, while the director components do not vanish. From the conjugation involution, the equation can be written as $s_m = \frac{1}{2}(\overset{o}{\varphi}_m + \overset{o}{\varphi}{}^*_m) = 0$. Consider an arbitrarily small increment in any of the solutions, say $\overset{o}{\varphi}_1 + \overset{o}{\delta} = \overset{o}{c} = s(m, r_s) + \delta s + (x(m, r_x) + \delta x)\check{\mathbf{e}}_x + (y(m, r_y) + \delta y)\check{\mathbf{e}}_y$, such that $s_m = \frac{1}{2}(\overset{o}{\varphi}_m + \overset{o}{\varphi}{}^*_m) = 0$ but $x_m \neq 0$ and $y_m \neq 0$. Points $\overset{o}{\varphi}_1 + \overset{o}{\delta}$ are in the neighborhood of $\overset{o}{\varphi}_1$. However, at the mth iteration, these points produce a scator $0 + x_m\check{\mathbf{e}}_x + y_m\check{\mathbf{e}}_y$ with divergent magnitude. ■

5. Nilpotent Points Iteration

Square nilpotent points are invariant points under the quadratic iteration, since $\overset{o}{\varphi}{}^2 = 0$, and the mapping $P(\overset{o}{\varphi})$ is then an identity $\overset{o}{\varphi} \mapsto \overset{o}{\varphi}{}^2 + \overset{o}{\varphi} = \overset{o}{\varphi}$. The critical orbit of a square nilpotent point $\overset{o}{\varphi}$ is $\{0, \overset{o}{\varphi}, \overset{o}{\varphi}, \ldots\}$. It is thus a preperiodic point with preperiod 1 and period 1. It is labeled as $\mathcal{M}_{1,1}$ in the notation of Misiurewicz points. It is then a preperiodic point that after one preperiod becomes a fixed point. From Lemma 1, nilpotent points $\overset{o}{\varphi} = \pm s \pm s\check{\mathbf{e}}_x \pm s\check{\mathbf{e}}_y$ lie on the intersection of the $s = \pm x$ and $s = \pm y$ planes, tilted at $\pm 45°$ with respect to the s axis. The projection of a point in the s, x plane onto a plane containing the s axis but inclined by θ in the x, y direction measured from the x axis is $x = r\cos\theta$ and $y = r\sin\theta$. For a plane $x = y$, $x = r\cos(\frac{\pi}{4}) = \frac{1}{\sqrt{2}}r = r\sin(\frac{\pi}{4}) = y$. The nilpotent lines $s = \pm x = \pm y$ in the s, r plane are thus $s = \pm\frac{1}{\sqrt{2}}r$. These two straight lines lie at $\frac{r}{s} = \arctan(\pm\sqrt{2}) \approx \pm 54.7°$ measured from the s axis, they are depicted in yellow in Fig. 5. These lines are superimposed over the confined **S** set drawn in white. Coloring is somewhat different from previous renderings to enhance the background. These lines are coincident with relevant features of the **S** set. On the negative side of the s axis, the largest bound region terminates at these lines that delineates an arrow-like head. On the positive s side, the nilpotent straight lines coincide with two of the large spikes coming out of the confined region. These lines should be in white since they are points within the bound set. However, they do not appear in the numerical iterative process because tiny departures in the rounding of $\sqrt{2}$ produce

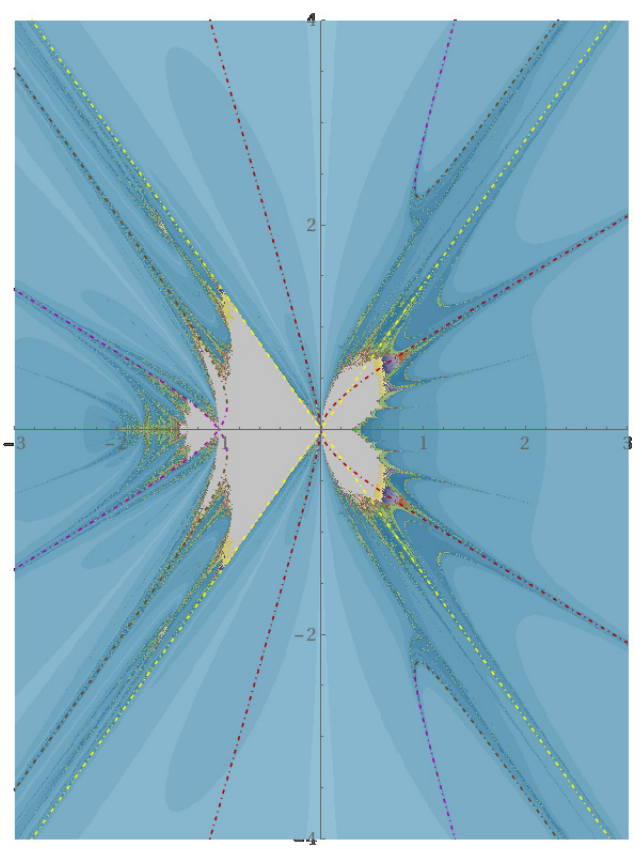

Fig. 5. Confined quadratic iteration in parameter space and square nilpotent curves for the first two iterations at the s versus $x = y$ plane. Square nilpotent points in yellow. Points such that $\overset{o}{\varphi}{}^2 + \overset{o}{\varphi}$ is square nilpotent are shown in red, magenta and brown. Dot dashed lines are drawn to see the underlying set points.

large magnitude values. The magnitude of nilpotent points is invariant under the quadratic mapping $\|\overset{o}{\varphi}^2 + \overset{o}{\varphi}\| = \|\overset{o}{\varphi}\| = \|\pm s \pm s\check{\mathbf{e}}_x \pm s\check{\mathbf{e}}_y\|$ and is equal to $\|\overset{o}{\varphi}\| = 2|s|$ in $1+2$ dimensions.

Lemma 3. *If m is the first positive integer such that $P_c^{\circ m}(0)$ is square nilpotent, the point $\overset{o}{\varphi} = \overset{o}{c}$ is preperiodic with preperiod 1 and period m in parameter space.*

Proof. The critical point for the quadratic mapping is zero[2] and is always the initial point in parameter space $\overset{o}{\varphi}_0 = 0$. The first iteration of the function is $P_c^{\circ 1}(0) = \overset{o}{c} = \overset{o}{\varphi}$, since $P_c^{\circ m}(0)$ is square nilpotent, $P_c^{\circ 1}(P_c^{\circ m}(0)) = \overset{o}{c} = \overset{o}{\varphi} = P_c^{\circ 1}(0)$. Then $P_c^{\circ 1+m}(0) = P_c^{\circ 1}(0)$ and thus $\mathcal{M}_{1,m} = \overset{o}{c} = \overset{o}{\varphi} : P_c^{\circ 1+m}(0) = P_c^{\circ 1}(0)$. ■

Consider now points such that $\overset{o}{\varphi}$ is not square nilpotent but $\overset{o}{\varphi}^2 + \overset{o}{\varphi}$ is square nilpotent, that is

$$(\overset{o}{\varphi}^2 + \overset{o}{\varphi})^2 = 0. \tag{14}$$

From Lemma 3, the preperiodicity is 1 and the periodicity 2. The critical orbit is $\{0, \overset{o}{\varphi}, (\overset{o}{\varphi}^2 + \overset{o}{\varphi}), \overset{o}{\varphi}, (\overset{o}{\varphi}^2 + \overset{o}{\varphi}), \ldots\}$. From Lemma 1, Eq. (14) is satisfied if the director components of $\overset{o}{\varphi}^2 + \overset{o}{\varphi}$ are equal to the scalar component or $\overset{o}{\varphi} = 0$. From (11a) and (11b), $s_2 = x_2$ requires that

$$s^2\left(1 - \frac{x^2}{s^2}\right)\left(1 - \frac{y^2}{s^2}\right) + s = 2sx\left(1 - \frac{y^2}{s^2}\right) + x$$

and $s_2 = y_2$,

$$s^2\left(1 - \frac{x^2}{s^2}\right)\left(1 - \frac{y^2}{s^2}\right) + s = 2sy\left(1 - \frac{x^2}{s^2}\right) + y.$$

These two equations have to be fulfilled simultaneously. Rewrite these equations as

$$(s^2 - x^2)(s^2 - y^2) + s^3 = 2sx(s^2 - y^2) + xs^2 \tag{15a}$$

$$(s^2 - x^2)(s^2 - y^2) + s^3 = 2sy(s^2 - x^2) + ys^2. \tag{15b}$$

Consider the equality between the RHS of these equations, $2sx(s^2 - y^2) + xs^2 = 2sy(s^2 - x^2) + ys^2$. This expression can be written as

$$2(x - y)s^2 + 2(x - y)xy + (x - y)s = 0. \tag{16}$$

Case 1. Nilpotent points with different initial director components. If $x \neq y$, divide (16) by $x - y$ to obtain $2s^2 + 2xy + s = 0$. Then solve for y,

$$y = -\frac{2s^2 + s}{2x} \tag{17}$$

and substitute in (15a),

$$(s^2 - x^2)\left(s^2 - \frac{(2s^2 + s)^2}{4x^2}\right) + s^3$$
$$= 2sx\left(s^2 - \frac{(2s^2 + s)^2}{4x^2}\right) + xs^2.$$

This expression can be written in polynomial form for x,

$$x^4 + (1 + 2s)x^3 - \left(2s^2 + 2s + \frac{1}{4}\right)x^2$$
$$- \left(s^2 + s + \frac{1}{4}\right)2s\,x + \left(s^2 + s + \frac{1}{4}\right)s^2 = 0.$$

Solutions are $x = (-(2s + 1) \pm \rho_1 \pm \rho_2)/4$, where

$$\rho_1 = \sqrt{2 + 8s + 4s^2} \quad \text{and}$$
$$\rho_2 = \sqrt{3 + 24s^2 - 2\rho_1 - 4s(\rho_1 - 5)}.$$

All four $\pm$ sign combinations produce the four different roots. The corresponding values for y are obtained from (17). These solutions do not lie in a plane but are (1D) curves embedded in 3D space.

Case 2. Nilpotent points with equal initial director components. The solutions with equal director components, $x = y$ substituted in Eq. (15a),

$$(s^2 - x^2)^2 + s^3 = 2sx(s^2 - x^2) + xs^2.$$

This equation is the projection of the equal directors nilpotent curve projected onto the s, x plane. It is interesting to notice that the constant magnitude curves $\varphi_0|s| = (s^2 + x^2)$ in the $s, x = y$ plane are two ellipses that when projected onto the s, x plane give two circles. In the $x = y$ plane, as we have mentioned before $x \to \frac{1}{\sqrt{2}}r$. The fourth

[2]We have not proved that zero is a critical point in the scator quadratic mapping and that it is the only critical point. In this sense, the proof is incomplete.

order polynomial in r is

$$r^4 - 2\sqrt{2}sr^3 - 4s^2r^2 + 2\sqrt{2}(2s^3 + s^2)r + (4s^4 + 4s^3) = 0. \tag{18}$$

The roots are

$$r_1 = -\sqrt{2}s, \quad r_2 = \left(\sqrt{2}s - \frac{4s^2}{\sigma} - \frac{\sigma}{3}\right),$$

$$r_{3,4} = \left(\sqrt{2}s + \frac{2s^2(1 \pm i\sqrt{3})}{\sigma} + \frac{(1 \mp i\sqrt{3})\sigma}{6}\right),$$

where

$$\sigma = 3^{\frac{1}{3}}(9\sqrt{2}s^2 + \sqrt{6}(27s^4 - 32s^6)^{\frac{1}{3}}).$$

A plot of these roots when they are real is shown in Fig. 6. The plane $x = -y$ also has equal director components' magnitude. The transformation $r \to -r$ produces curves r_5 to r_8 that are the negatives of r_1 to r_4. The eight curves arising from all roots are plotted together on the right side of Fig. 6. The root r_2 (red in Figs. 5 and 6) is always real and is coincident in the $s < 0$ semiplane with the larger whiskers (see also Fig. 8) of the bound set coming off from zero. On the positive s side, the r_2, r_6 nilpotent roots coincide with two other large spikes coming out of the confined region. The roots r_3 and r_7 cross at $r = 0$ (yellow curves). If we evaluate s at $r = 0$ from (18), either $s = 0$ or $s = -1$. Since $P^{\circ 1}(\overset{o}{\varphi}) = \overset{o}{\varphi}^2 + \overset{o}{\varphi}$ is square nilpotent, from Lemma 3, the points $\overset{o}{\varphi}$ have periodicity 2. This result is consistent with the well known periodicity of points lying on the real axis where the period 2 iteration point is -1. On the $s < 0$ semispace, the r_3 and r_7 curves (magenta curves in Figs. 5 and 6) delineate a smaller arrow-like head whose tip lies at -1. The remaining part of these curves together with the r_4 and r_8 curves (brown curves in Figs. 5 and 6) delineate the tail of the largest arrow. The r_3, r_4 and r_7, r_8 curves in the $s > 0$ semispace are well off the main cardioid region. These curves are coincident with some of the long range curved spikes produced in the numerical evaluation.

5.1. *Upper bound*

The **S** set, following Douady [Douady & Hubbard, 1984], has been defined by the set of points whose magnitude does not tend to infinity for any number of iterations [Eq. (9)]. In order to evaluate the points in the set numerically, the divergence condition has to be cast in terms of an upper bound b,

$$\mathbf{S}_a = \{\overset{o}{c} \in \overline{\mathbb{E}}^{1+2} : \forall\, m \in \mathbb{N}, \exists\, b \in \mathbb{R}, \|P_c^{\circ m}(0)\|^2 \leq b\}. \tag{19}$$

In complex dynamics it suffices to consider an upper bound of 4 because any complex number with magnitude larger than 2 necessarily diverges

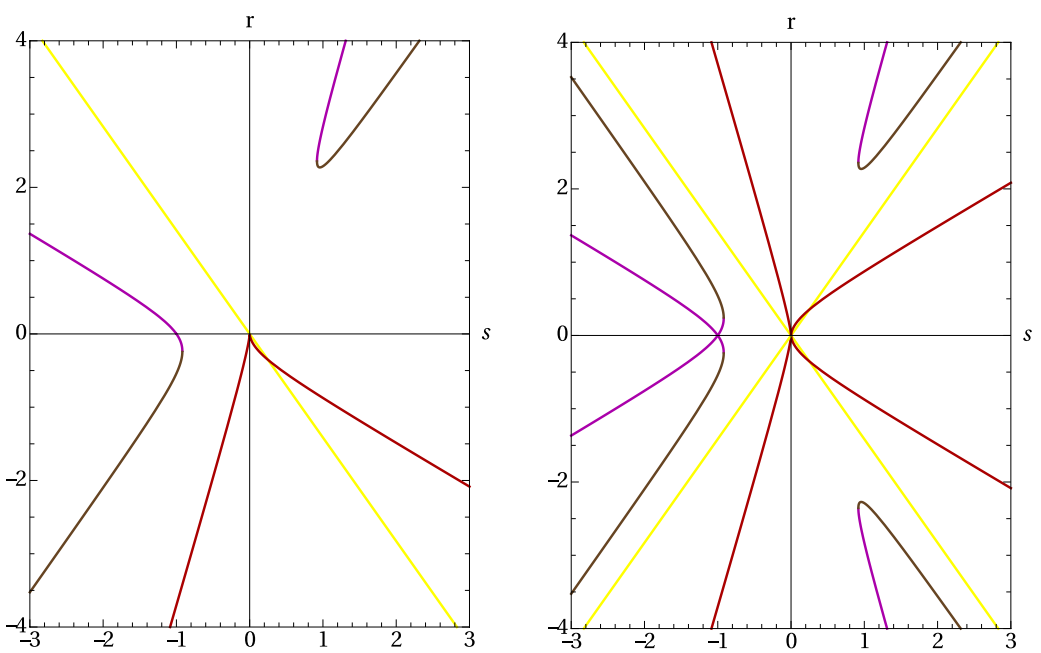

Fig. 6. Curves produced by roots r_1 (yellow), r_2 (red), r_3 (magenta) and r_4 (brown) of the square nilpotent scator on the second iteration. On the right all eight roots are shown.

as the number of iterations increases. The question of course arises regarding an upper bound in imaginary scator algebra.

Lemma 4. *There is no upper bound b to the scator squared magnitude, such that scators with magnitude larger than b diverge under the quadratic iteration in parameter space.*

Proof. Suppose that there is an upper bound b so that for any bound scator point $\overset{o}{c}$, $\|P_c^{\circ m}(0)\|^2 \leq b$. The square magnitude of the scator $\overset{o}{c} = P_c^{\circ m}(0)$ is at most b. Such scator can be constructed with components $\overset{o}{c} = \frac{\sqrt{b}}{2} + \frac{\sqrt{b}}{2}\check{\mathbf{e}}_x + \frac{\sqrt{b}}{2}\check{\mathbf{e}}_y$, so that its square magnitude is b. Consider a scator $\overset{o}{B} = \frac{\sqrt{B}}{2} + \frac{\sqrt{B}}{2}\check{\mathbf{e}}_x + \frac{\sqrt{B}}{2}\check{\mathbf{e}}_y$ with $B > b$. This scator is square nilpotent, and thus with preperiod 1 and thereafter a fixed point with square magnitude B. Thus it does not diverge. But $B > b$ and therefore b is not an upper bound. ■

It could be possible that considerable differences arise when the bound set is evaluated with different upper bounds. In Fig. 7, on the left, the scator square magnitude was compared with $\|P_c^{\circ m}(0)\|^2 < 400$, that is, the iteration process is suspended if the scator magnitude is greater than 20. On the right, the scator square magnitude was compared with $\|P_c^{\circ m}(0)\|^2 < 4$, the usual bailout condition where the iteration process is stopped (scator magnitude greater than 2). The bound set is almost identical in either case. The outer escape iso-surfaces are different because, in one case, the first iteration is a circle of radius 20 whereas in the other it is a circle ten times smaller. The difference between the rims of these iso-surfaces becomes smaller as they approach the boundary of the confined set in the iteration process.

The proof of Lemma 4 relies on the fact that no upper bound exists for nilpotents. An interesting plane to look for differences is then the $x = y$ plane where nilpotent fixed points exist as well as higher order preperiodic points with larger periodicity. Figure 8 shows a detailed region of this plane where the most relevant differences in the bound set were observed. The bound sets are again quite similar. Nonetheless, the spikes close to the scalar axis are somewhat cropped when $b = 4$ compared with those obtained when $b = 400$. It must be stressed that nilpotent points are always bound and should come out in white. However, they are easily missed by the numerical evaluation mesh. Points near to nilpotent values diverge after a few iterations. The set $\mathbf{S}_a$ defined in terms of an upper bound (19), is thus only approximately correct because it misses some of the bound points.

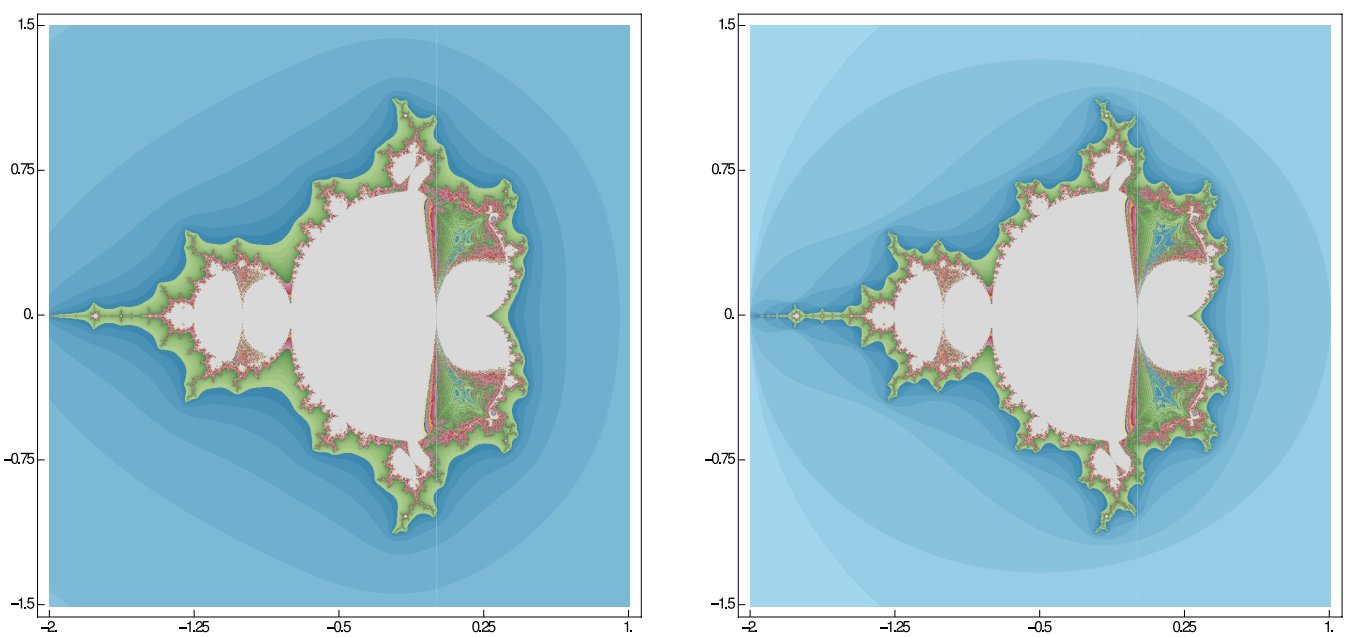

Fig. 7. Comparison of sets in the $(s; x, 10^{-7})$ plane, produced with different upper bound b, $\|P_c^{\circ m}(0)\|^2 < 400$ on the left and $\|P_c^{\circ m}(0)\|^2 < 4$ on the right. The numerical estimate of the bound region drawn in white is nonetheless very similar. Some differences arise in the outer escape iso-surfaces.

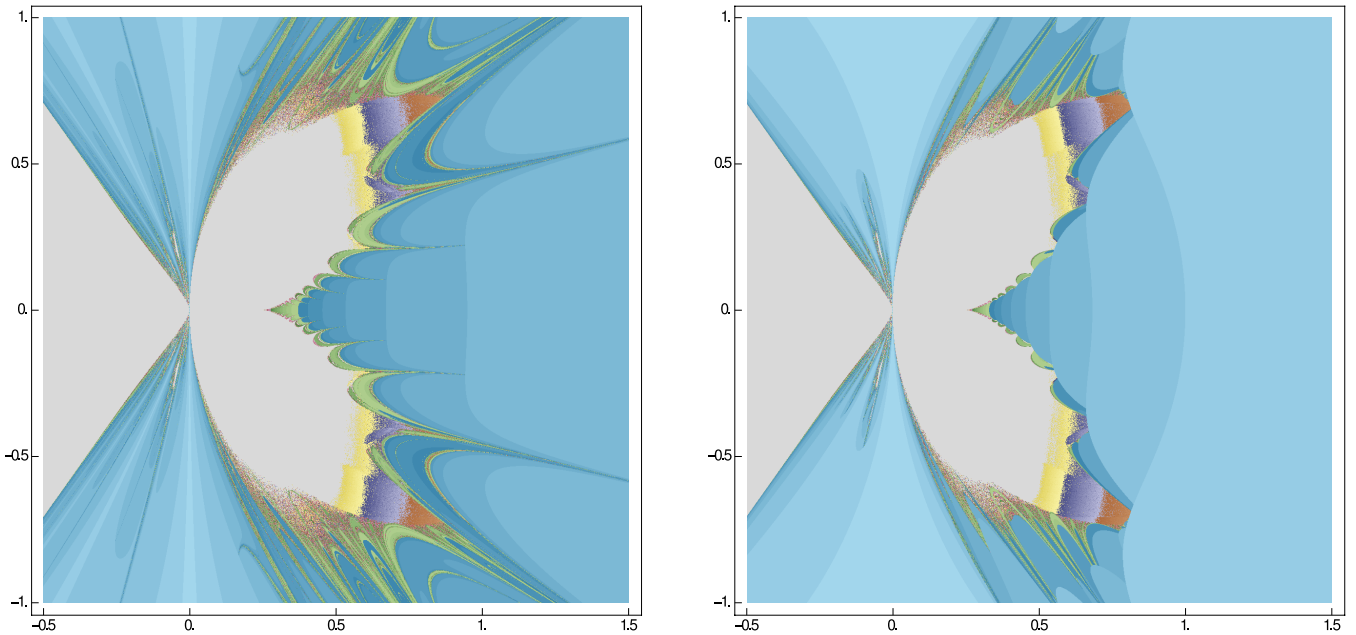

Fig. 8. Comparison of sets in s, r plane, $r = \sqrt{2}x = \sqrt{2}y$, produced with different upper bound b, $\|P_c^{\circ m}(0)\|^2 \leq 400$ on the left and $\|P_c^{\circ m}(0)\|^2 \leq 4$ on the right. The bound region drawn in white is still quite similar. Some of the spikes are trimmed when the magnitude limit is set to 4.

5.2. *Scator versus Euclidean magnitude*

Definitions of the **S** set (9) and (19) make decisive use of the scator magnitude. Recall that in complex algebra, it does not matter whether the comparison is performed with the magnitude or either the real or imaginary parts of the complex number. All three quantities either diverge or are all bound. In contrast, the condition is critical in hyperbolic numbers' algebra [Pavlov *et al.*, 2009]. The real and imaginary parts of the hyperbolic number may increase indefinitely while their square difference remains bounded [Fernández-Guasti, 2014]. In imaginary scator algebra, the term involving the inverse squared of the scalar component $\frac{x^2y^2}{s^2}$, plays a crucial role in establishing the divergent magnitude vicinity of periodic points, as we saw in Sec. 4. Let us evaluate the relevance of the scator magnitude form in the numerical evaluation regarding the so-called "bailout" condition. The condition $\|P_c^{\circ m}(0)\|^2 \leq b$ with the scator magnitude form is $s_m^2 + x_m^2 + y_m^2 + \frac{x_m^2 y_m^2}{s_m^2} \leq b$, while the condition established with the Euclidean norm is $s_m^2 + x_m^2 + y_m^2 \leq b$. The numerical evaluation of the bound sets with these two conditions are compared in Fig. 9. The square imaginary scator metric is always larger than the Euclidean metric by a factor of $\frac{x_m^2 y_m^2}{s_m^2}$ in 1+2 dimensions. In the first iteration, the scator is $s + x\check{\mathbf{e}}_x + y\check{\mathbf{e}}_y$. The Euclidean magnitude is a sphere and its intersection with the $y = 0.02$ plane gives a circle. This outermost circle is shaded in light blue in Fig. 9 (right). On the other hand, the scator magnitude involves the extra factor $\frac{x^2y^2}{s^2}$. This quantity becomes very large when s is close to zero while x, y are finite. For this reason, the outermost contour in Fig. 9 (left) is cleaved at the $s = 0$ plane. This cleavage vanishes if the hyperplane y is zero (or the hyperplane x is zero) because then the term involving the inverse squared scalar component vanishes. Nonetheless, at the next iteration, even the Euclidean magnitude $s_2^2 + x_2^2 + y_2^2$ contains terms with inverse squared scalar terms, as may be seen from (11a) and (11b). This contour corresponds to the next shade of blue in the Fig. 9 (right). It already shows a cleavage at the origin. However, no cleavage is observed at -1 for the second iteration while the scator magnitude in Fig. 9 (left) already has a cleavage at -1 and an additional cleavage at zero. As higher order iterations are considered, the contours with the Euclidean metric seem to lag one behind the scator metric. At any rate, the scator magnitude is the appropriate metric for scator algebra since it is the one that is derived from the second order involution of the algebra.

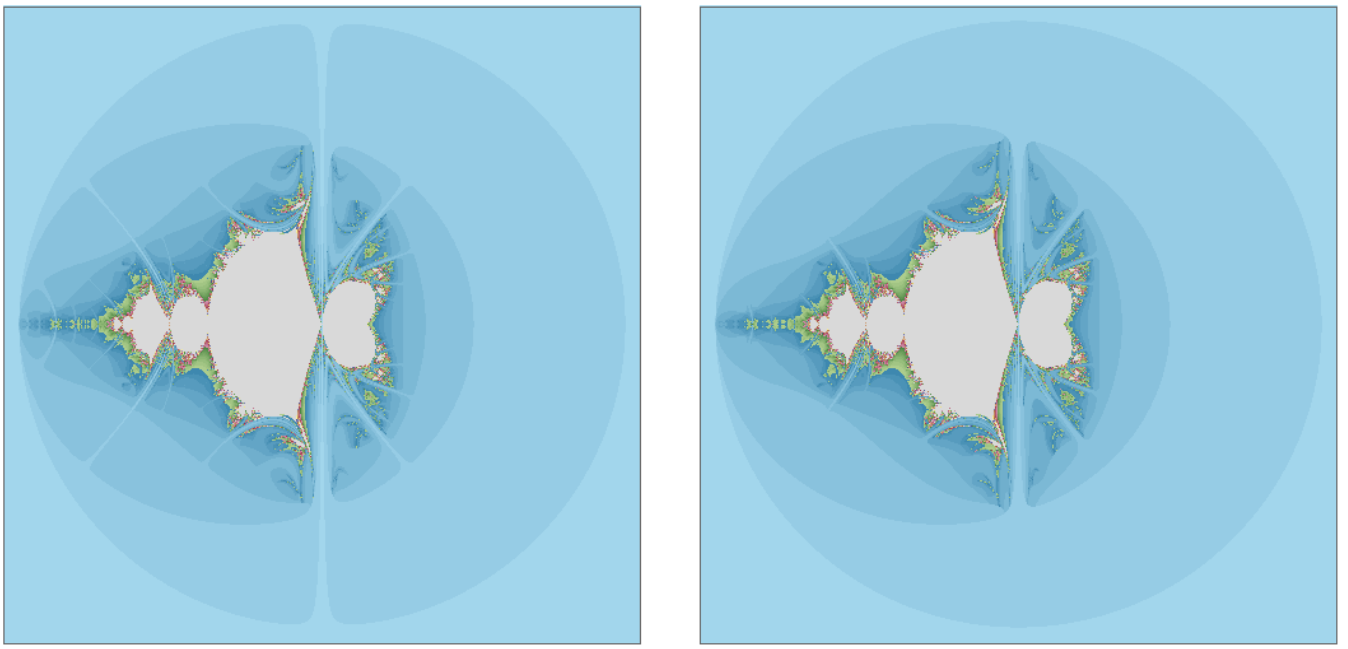

Fig. 9. Scator versus Euclidean, $s; x$ plane at hyperplane $y = 0.02$. Bound set colored in white. Evaluation with scator magnitude condition (left) and with Euclidean magnitude (right).

6. Symmetries of the S Set in Three Dimensions

The bound **S** set in parameter space in $\overline{\mathbb{E}}^{1+2}$, is a set of points in a three-dimensional volume. In Fig. 10, the image of a three-dimensional representation of the **S** set is shown. This 3D version was produced with P. Willenius' extraordinary rendering program [Willenius, 2013, v.2.0.1]. Thirteen iterations were performed on each point. The coloring is due to the value of the components in the last iteration, the scalar, x and y director values proportional to red, green and blue respectively (s_{13} {red}; x_{13} {green}, y_{13} {blue}). The image is extremely intricate and somewhat sensitive to drawing parameters. The M-set silhouette should be visible but it is not. The reason is two-fold: On the one hand, there are regions of the boundary surface with $x > 0$ that overshadow the $x = 0$ plane. On the other hand, the mesh in the $\check{\mathbf{e}}_x$ hypercomplex axis is evaluated in 500 layers from -0.97 to 1.79. As we have shown in Sec. 3, it suffices that the mesh misses the $x = 0$ plane even by tiny values (i.e. 10^{-7}) for the set to be considerably deformed. Some regions in the set, such as the M-set near the $s = 0$ plane are extremely thin. When a few iterations are evaluated, these regions are partially "caught" within the bound criterion. However, as the number of iterations increases, if the mesh points do not intersect the thin bound regions they become lost. To retain them, a much finer mesh is required with the concomitant increase in the number of operations. Figure 10 already involves the

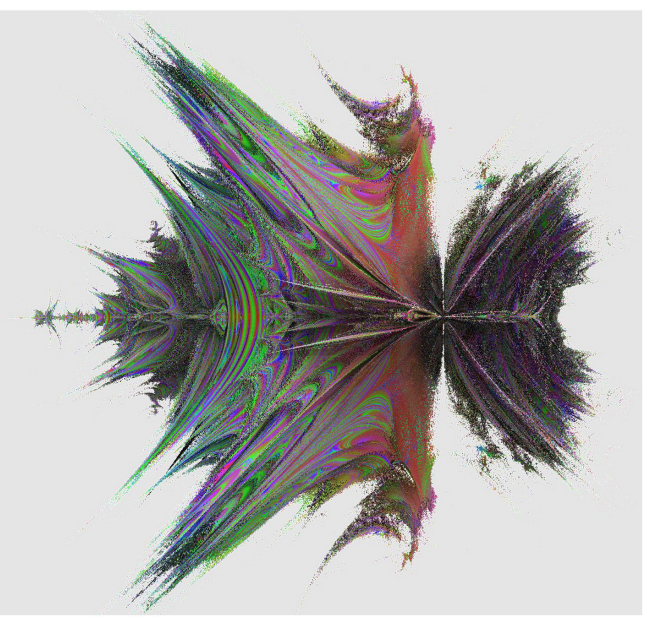

Fig. 10. Three-dimensional rendering of the **S** set in $\overline{\mathbb{E}}^{1+2}$ viewed from the first director hypercomplex axis $\check{\mathbf{e}}_x$. A maximum of 13 iterations per point were performed. The abscissa represents the scalar (or real) s axis, while the ordinate depicts the second director hypercomplex axis $\check{\mathbf{e}}_y$.

evaluation of 1.805×10^9 points ($1900 \times 1900 \times 500$). A possibility, in order to visualize features that are revealed with different resolutions and iterations, is to superimpose various images with varying degree of transparency.

The 3D set is squeezed at $s = 0$. The lack of bound points in the vicinity of the $s = 0$ plane is due to the divergent vicinity $\mathbf{R}_s$ described in (7). Other divergent planes are not clearly seen because they have curved surfaces, as evinced from those depicted in Fig. 2, that produce divergent magnitude points in the second iteration. On the far left, there is a hint of a self-similar smaller version of the larger set.

The two hypercomplex axes are entirely equivalent, thus there is invariance upon interchange of the x and y variables. Therefore, there must be symmetry upon reflection in the x, y plane as is indeed observed. The x hypercomplex director component is an odd function of x, thus upon iteration, the function will be equal but with opposite sign under the transformation $x \to -x$. An equivalent reasoning leads to the $y \to -y$ symmetry about the ordinate hypercomplex axis that is observed in Fig. 10. The transformation $s \to -s$ does not have a well defined parity for the resultant scalar term $s^2 + x^2 + y^2 + \frac{x^2y^2}{s^2} + s$. Thus, the iterated map is asymmetric with respect to the scalar axis inversion.

6.1. *Visualization and notation*

An infinite number of planes can intersect the 3D **S** set. The M-set is only one of these many intersections at either the $x = 0$ or $y = 0$ plane. Moreover, the many Julia sets on the complex plane become 3D sets in $\mathbb{E}^{1+2}$, each of them with the possibility of many intersections with 2D planes. The following notation has been used by the author to label the sets depicted on different planes:

c2i <u>c</u>onfined {**2**} quadratic <u>i</u>terations, (that can be generalized to **cpi** for a pth power polynomial or $p \to$ *func* for other *func*tion's mappings)

- followed by **0** if the initial value of the variable is set to zero (set depicted in parameter space) or the initial value $(s_i; x_i, y_i)$ at which the constant is fixed (set depicted in dynamical space).
- followed by the number system: $\mathbb{R}$ real, $\mathbb{C}$ complex, $\mathbb{H}$ hyperbolic, $\mathbb{E}_-^{1+n}$ imaginary or $\mathbb{E}_+^{1+n}$ real scators (in $1 + n$ dimensions), etc.
- followed, if necessary, by the viewpoint or plane $(p_0; p_1, p_2)$ that is being depicted.
- in 3D renderings, fractal location and viewpoint are required.

Thus, the Mandelbrot set in the complex plane is labeled **c2i0**$\mathbb{C}$, whereas the filled-in Julia set K_c in the complex plane for the point $z = a + ib$ is labeled **c2i**$(a, b)\mathbb{C}$. Since imaginary scators with only one component are identical to complex numbers, the sets **c2i0**$\mathbb{C}$ and **c2i0**$\mathbb{E}_-^{1+1}$ are equivalent. The **S** set in parameter space for imaginary scators in $1 + 2$ dimensions presented here, according with the proposed notation, is labeled **c2i0**$\mathbb{E}_-^{1+2}$. The sets of Figs. 1, 4 and 7 are labeled **c2i0**$\mathbb{E}_-^{1+2}(s; x, 10^{-7})$, while the set of Fig. 9 is labeled **c2i0**$\mathbb{E}_-^{1+2}(s; x, 10^{-2})$. The sets in Figs. 5 and 8 are labeled **c2i0**$\mathbb{E}_-^{1+2}(s; r/\sqrt{2}, r/\sqrt{2})$. The 3D rendering of Fig. 10 is labeled **c2i0**$\mathbb{E}_-^{1+2}(0; 0, 0)(0; 6, 0)$.

7. Conclusions

The **S** set in $\overline{\mathbb{E}}_-^{1+2}(s; x, y)$ has been defined in parameter space in terms of scators whose magnitude does not tend to infinity under the quadratic iteration. Imaginary scator algebra is a finite dimensional algebra with the peculiarity that the scator product is commutative but does not distribute over addition. It is equipped with an order parameter that in addition to the sum of the squared components also involves terms with the inverse squared of the scalar component. The quadratic mapping has been justified on two grounds: (i) The scator square function is defined by the scator product operation of an element with itself, and (ii) if the argument of the square function is multiplied by a scalar, the outcome is equivalent to multiplication by the square of the scalar (Lemma 2). The 3D **S** set exhibits a rich and intricate boundary not found in other higher dimensional generalizations of the Mandelbrot set.

Evaluation of the **S** set at a constant but small value of the second director hypercomplex variable ($y = 10^{-7}$) reveals a distribution somewhat similar to the M-set but with the main cardiod and the bulbs squeezed at their centers. To explain this behavior, the extended scator set $\overline{\mathbb{E}}_-^{1+2}$ that includes the points at infinity has been introduced. Besides the usual points whose components tend to infinity, this set also contains scator elements with null scalar and finite director components

[$\mathbf{R}_s$ set, Eqs. (6) and (7)]. This situation motivated the definition of points that have a divergent vicinity (Definition 2.1). Proposition 1, then established that periodic points with period m have a vicinity that maps onto the divergent magnitude set $\mathbf{R}_s$ in the mth iteration. There is no counterpart to this *periodic point–divergent vicinity* behavior in two dimensions. It is a consequence of the non-Euclidean magnitude of scator elements that becomes relevant only in dimensions higher than two. These results allow us to explain the squeezing at the centers of the bulbs where the mth periodic point is located. Examples have been presented for the first three iterations.

Square nilpotent elements have been characterized in Lemma 1. Thereafter, we have shown in Lemma 3, the preperiodicity of points that are square nilpotent on the mth iteration. This result has been illustrated with the square nilpotent curves obtained on the second iteration at the plane with equal initial director components. With the preceding results, we have shown in Lemma 4, that there is no upper bound to the scator magnitude such that scators with larger magnitude diverge under the square iteration. Thus, the definition of a $\mathbf{S}_a$ set in terms of an upper bound (19) is not equal to the strict definition (9), although it is certainly useful for numerical evaluations.

Some features and elementary symmetries of the three-dimensional $\mathbf{S}$ set have been described. The symmetry between the two director hypercomplex axes produces indistinguishable copies of the M-set in the s, x and s, y hyperplanes. In contrast, recall that other algebraic generalizations to higher dimensions do not exhibit identical properties when hypercomplex components are interchanged. Real and complex algebra are embedded in imaginary scator algebra; $\mathbb{R}$ and $\mathbb{C}$ are thus subsets of the $\mathbb{E}_{-}^{1+2}$ imaginary scator set. Therefore, features of the M-set such as the period-doubling cascade leading to the Myrberg–Feigenbaum point or the one to one correspondence with the bifurcation diagram of the logistic map are also present in the imaginary scator set. Different regions of the $\mathbf{c2i0}\mathbb{E}^{1+2}(s; x, y)$ set reveal extraordinary structures that we have only glimpsed at in an unsystematic fashion. Self-similarity is present in the 3D structure. Powerful rendering techniques are required to visualize the intricacies of these higher dimensional sets.

Acknowledgments

I am grateful to A. Vilchis, F. Zaldívar for their critical reading of the early scator algebra manuscripts and J. L. del Río for a lifelong shared interest in fractal structures.

References

Araki, Y. [2006] "Materializing 3D quasi-Fuchsian fractals," *Forma* **21**, 19–27.

Aron, J. [2009] "The Mandelbulb: First 'true' 3D image of famous fractal," *New Scientist* **204**, p. 54.

Bedding, S. & Briggs, K. [1995] "Iteration of quaternion maps," *Int. J. Bifurcation and Chaos* **5**, 877–881.

Blackledge, J. [2002] *Fractal Geometry*: *Mathematical Methods*, *Algorithms*, *Applications* (Woodhead Publishing).

Blanchard, P. [1984] "Complex analytical dynamics on the Riemann sphere," *Bull. Amer. Math. Soc.* **11**, 85–141.

Bonzini, P. [2010] "To quaternions and back," http://www.fractal.org/mbulb-paolo-bonzini.pdf.

Catoni, F., Boccaletti, D., Cannata, R., Catoni, V., Nichelatti, E. & Zampetti, P. [2008] *The Mathematics of Minkowski Space-Time*, Frontiers in Mathematics (Birkhäuser-Verlag).

Cheng, J. & Tan, J.-R. [2007] "Generalization of 3D Mandelbrot and Julia sets," *J. Zhejiang Univ. Sci. A* **8**, 134–141.

Douady, A. & Hubbard, J. H. [1984] "Exploring the Mandelbrot set," Tech. Rep., Université Paris Sud.

Fernández-Guasti, M. & Zaldívar, F. [2013a] "A hyperbolic nondistributive algebra in 1 + 2 dimensions," *Adv. Appl. Clifford Algebr.* **23**, 639–653.

Fernández-Guasti, M. & Zaldívar, F. [2013b] "An elliptic nondistributive algebra," *Adv. Appl. Clifford Algebr.* **23**, 825–835.

Fernández-Guasti, M. [2014] "An intrinsically three dimensional fractal," *Int. J. Bifurcation and Chaos* **24**, 1430017-1–13.

Gomatam, J., Doyle, J., Steves, B. & McFarlane, I. [1995] "Generalization of the Mandelbrot set: Quaternionic quadratic maps," *Chaos Solit. Fract.* **5**, 971–986.

Helmstetter, J. & Micali, A. [2008] *Quadratic Mappings and Clifford Algebras* (Birkhäuser Basel).

Kantor, I. L. & Solodovnikov, A. S. [1989] *Hypercomplex Numbers* (Springer-Verlag).

Nascimento-Baptista, A., Ramos, C. C. & Martins, N. [2012] "Iteration of quadratic maps on matrix algebras," *Int. J. Bifurcation and Chaos* **22**, 1250150-1–7.

Pavlov, D. G., Panchelyuga, M. S., Malykhin, V. A. & Panchelyuga, V. A. [2009] "On fractality of Mandelbrot and Julia sets on double-numbers plane,"

Hypercomplex Numbers in Geometry and Physics **6**, 135–145.

Rama, B. & Mishra, J. [2011] "Generation of 3D fractal images for Mandelbrot set," *Proc. 2011 Int. Conf. Communication, Computing & Security*, ICCCS '11 (ACM, NY, USA).

Sanderson, K. [2009] "2009 Gallery: Images of the year," *Nature* **462**, 972–977.

White, D. & Nylander, P. [2009] "Triplex algebra," http://www.fractalforums.com/theory/triplex-algebra/.

Willenius, P. [2013] "Fractrace," https://github.com/trafassel/Gestaltlupe.